

## Non-thermal evolution of dense plasmas driven by intense x-ray fields

Shenyuan Ren<sup>1,5</sup>, Yuanfeng Shi<sup>1</sup>, Quincy Y. van den Berg<sup>1</sup>, Muhammad F. Kasim<sup>1</sup>, Hyun-Kyung Chung<sup>2</sup>, Elisa V. Fernandez-Tello<sup>3</sup>, Pedro Velarde<sup>3</sup>, Justin S. Wark<sup>1</sup> & Sam M. Vinko<sup>1,4</sup>✉

The advent of x-ray free-electron lasers has enabled a range of new experimental investigations into the properties of matter driven to extreme conditions via intense x-ray-matter interactions. The femtosecond timescales of these interactions lead to the creation of transient high-energy-density plasmas, where both the electrons and the ions may be far from local thermodynamic equilibrium. Predictive modelling of such systems remains challenging because of the different timescales at which electrons and ions thermalize, and because of the vast number of atomic configurations required to describe highly-ionized plasmas. Here we present CCFLY, a code designed to model the time-dependent evolution of both electron distributions and ion states interacting with intense x-ray fields on ultra-short timescales, far from local thermodynamic equilibrium. We explore how the plasma relaxes to local thermodynamic equilibrium on femtosecond timescales in terms of the charge state distribution, electron density, and temperature.

<sup>1</sup>Department of Physics, Clarendon Laboratory, University of Oxford, Parks Road, Oxford OX1 3PU, UK. <sup>2</sup>Korea Institute of Fusion Energy, Daejeon 34133, Republic of Korea. <sup>3</sup>Instituto de Fusión Nuclear, Universidad Politécnica de Madrid, José Gutiérrez Abascal 2, 28006 Madrid, Spain. <sup>4</sup>Central Laser Facility, STFC Rutherford Appleton Laboratory, Didcot OX11 0QX, UK. <sup>5</sup>Present address: Beijing Jiaotong University, Beijing, China. ✉email: [sam.vinko@physics.ox.ac.uk](mailto:sam.vinko@physics.ox.ac.uk)

Experiments carried out at x-ray free-electron lasers (FELs) over the past decade have shown how intense x-ray fields can produce well-characterised plasmas at high temperatures and densities via isochoric x-ray photoabsorption<sup>1–4</sup>. This approach has proven valuable in providing access to physical properties and atomic processes in warm dense matter, of importance to applications across plasma physics<sup>5–7</sup>, astrophysics and planetary studies<sup>8,9</sup>, and fusion energy science<sup>10</sup>. Experimentally, the systems produced are typically studied via x-ray emission or inelastic scattering spectroscopy<sup>2,11</sup>, while the theoretical description is provided by time-dependent atomic kinetics calculations<sup>4,12</sup>.

Because of the short pulse duration of FEL x-ray sources, on the order of 100 fs, the time evolution of the ionisation and ionic charge state populations must be modelled directly via collisional-radiative rate equations, and local thermodynamic equilibrium (LTE) cannot be assumed – such models are thus called non-LTE. In contrast, these same timescales are typically long for the purposes of electron equilibration, and the free electron distribution is often modelled using a Maxwell-Boltzmann distribution function at some evolving (but instantly equilibrating) electron temperature and density. Being able to replace the time evolution of the full electron distribution function by a time-dependent temperature and density is convenient computationally as it leads to a substantial simplification in modelling complexity, but it also carries significant physical implications. For one, the shape of the electron distribution determines multiple properties that govern the evolution of the atomic kinetics, including photoemission and collisional ionisation rates; these can be altered significantly by non-thermal electron distributions.

The importance of properly accounting for electron equilibration dynamics was demonstrated in early ultrafast experiments at the FLASH FEL with XUV pulses a few tens of fs in duration. There, the electron relaxation time was comparable to the typical lifetime of radiative decay, leading to fluorescence emission from a seemingly cold (non-equilibrated) distribution, alongside a bremsstrahlung emission spectrum arising from the non-thermal electrons consistent with a 20-times higher effective temperature<sup>13,14</sup>. The contribution from non-thermal electrons to the total emission spectrum is amplified in such experiments due to the combination of low-energy XUV photoexcitation (<100 eV) and short pulse lengths. In contrast, similar effects are expected to be less important at harder x-ray photon energies (>1 keV) and for typical x-ray pulse durations of 60–80 fs<sup>1,15</sup>. Nevertheless, experimental access to both high x-ray intensities and ultra-short pulse lengths (<10 fs) will undoubtedly lead to novel x-ray matter interaction regimes where non-thermal electron dynamics dominates the plasma evolution, even on x-ray emission and scattering timescales. This poses a challenge to established modelling approaches, but also provides new opportunities to study ultrafast electron equilibration in a hot-dense plasmas experimentally in situ.

The effect of non-thermal electrons in extreme conditions can be modelled in various ways, and efforts have been made in both x-ray Thomson scattering<sup>16</sup> and x-ray emission spectroscopy investigations via non-thermal atomic kinetics<sup>17</sup>. A kinetic modelling addition to the particle-in-cell (PIC) simulation suite PICLS<sup>18,19</sup> allowed for the inclusion of self-consistent radiation transport, photoionization and Auger electron transport, enabling a full kinetic simulation of XFEL-driven plasmas<sup>20</sup>. While PIC-based models are very capable in capturing the evolution of the electron distribution in time and in space, they lack the full predictive capability for detailed x-ray emission spectroscopy. In contrast, non-thermal collisional-radiative codes deploying Fokker-Planck<sup>17,21</sup> or Boltzmann solvers<sup>22</sup> to treat non-Maxwellian electrons are able to treat a vast number of ionic

charge configurations, essential for predicting x-ray emission, and allow us to investigate the effect of non-thermal distributions on spectroscopic experiments at FEL facilities.

It is in this context that we present CCFLY, a non-thermal, non-LTE collisional radiative code, designed to model the time-dependent evolution of both electron distributions and ion states interacting with intense x-ray fields on ultra-short timescales. The code is an evolution of the SCFLY suite<sup>12,23</sup>, itself based on the FLYCHK code<sup>24</sup>, which has proven successful in modelling and interpreting an array of x-ray FEL experiments over the past decade<sup>4</sup>. CCFLY allows us to model the plasma evolution by tracking arbitrary electron distribution functions during the atomic-kinetics calculation, foregoing the need to assume a Maxwellian distribution for the free electrons. More precisely, the Fokker-Planck numerical framework is used to describe the evolution of the electron distribution during the elastic electron-electron collisions and account for the electrons released or absorbed during inelastic electron-ion interactions. A self-consistent method is deployed to compute the density and energy balance of the free-electron population together with the ion population dynamics in a partially ionised dense plasma. Thus, it becomes possible for us to investigate ionisation dynamics in both equilibrated and non-equilibrated systems at high density. We note here that while CCFLY tracks the time-evolution of the electron distribution and of the ionic charge states, it does not explicitly take into account the motion of ions. As is normally the case in atomic-kinetics modelling, there is no molecular dynamics, and the ions have no associated kinetic energy (and thus no temperature). This is adequate to describe the evolution of x-ray-irradiated samples on femtosecond timescales, but starts to break down as the ions are heated. However, ion heating takes place on longer picosecond timescales, normally dictated by electron-phonon coupling dynamics<sup>25–28</sup>.

We use CCFLY to study the effect of non-thermal electrons in Al and Mg plasmas irradiated by soft x-ray pulses with characteristics achievable at current x-ray FEL facilities. We study both normal isochoric heating experimental setups, where the x-ray photon energy is chosen to be higher than the ionisation threshold of several ionic charge states, and resonant pumping configurations where the x-ray pulse is tuned to a specific bound-bound atomic resonance. In both cases we find that non-thermal electron processes become important for short pulse durations and at high intensities. We quantify the regimes for which instantaneous thermalisation assumptions hold, and provide a more rigorous justification for the modelling assumptions employed in previous x-ray spectroscopy experiments at the Linac Coherent Light Source (LCLS)<sup>1,4,5,15,26,29–36</sup>. In particular, we aim to provide a rigorous evaluation of non-thermal electron effects on x-ray isochoric heating experiments where electron temperatures typically reach 50–200 eV. Because solid-density metals predominantly have Fermi energies of <10 eV, this regime justifies the use of classical statistics for all but the earliest times in the x-ray-matter interaction process, which in turn allows for a direct comparison with previous simulation work. The inclusion of Fermi-Dirac statistics for the accurate modelling of temperatures below ~10 eV will be the subject of future work.

## Results

The atomic kinetics collisional-radiative modelling approach is a well-established way to track the evolution of the charge states in the plasma as it interacts with intense x-ray fields<sup>37</sup>. The model is zero dimensional, and assumes ions in various ionisation states interacting with a classical free electron gas (the ionised free electrons), the density of which is constrained by the requirement for the overall plasma to be charge-neutral. The transitions

between various ion states are driven by electron collisional and atomic processes, but are also mediated by the x-ray photon field. The evolution of the system is described in terms of the changes in the relative population density of each ionic charge state, and in the distribution function of the free electrons. More details on the theory used for the simulations are provided in the Methods section.

We used superconfigurations to represent the states in our atomic kinetics modelling, and a more detailed relativistic configurations atomic model for the spectral synthesis. The energy levels, statistical weights, and radiative data required to produce the frequency-dependent emissivities and opacities were calculated using the DHS code<sup>38</sup>. Population distributions of relativistic configurations belonging to a super-configuration (or to a super-shell) were determined by Boltzmann statistics as a function of electron temperature<sup>4,24,39</sup>.

The effect of continuum lowering, where the binding energies of atomic states are lowered due to high electron and ion density, is accounted for in the atomic kinetics calculation via an ionisation potential depression (IPD) model. While the CCFLY code supports multiple IPD models, for the simulations presented here we have used the Ecker-Kröll model<sup>40</sup> to make the results directly comparable to previously published work.

In the following we call the model thermal if we assume that the electron distribution function is Maxwellian, uniquely described by some electron density and temperature. When energy enters the system, for example via x-ray photoabsorption, the temperature and density are instantaneously equilibrated at each time step. In contrast, if a thermal electron distribution cannot be assumed, then the change in the electron distribution needs to be modelled explicitly for all electron energies. To accomplish this we use the Fokker-Planck model. We refer to this situation as the non-thermal case. Note that the ion population is never assumed to be thermal, and the time-dependent modelling of the charge state evolution is non-LTE for both the thermal and non-thermal simulation approaches.

**Non-thermal electrons in x-ray isochoric heating.** The CCFLY code allows us to investigate the detailed evolution of the electron distribution function in an isochoric heating experiment at an x-ray FEL. In particular, we are interested in exploring what role non-thermal electrons play in the atomic kinetics of the system, and wish to assess the range of validity of the instantaneous electron thermalisation assumption commonly used in the modelling and in the interpretation of experimental results.

From optical laser-plasma experiments it is well known that even small fractions of hot, non-thermal electrons can significantly alter the emission spectrum from a plasma source<sup>41,42</sup>. However, unlike in optical laser-plasma interactions where electrons with energies ranging from several 10's of keV to MeV can be created relatively efficiently through various laser-plasma acceleration mechanisms, here the hot electrons are created purely by atomic processes within the plasma volume. Our hot electron distribution is thus well defined in space, time, and energy, but is also far less energetic – limited to 1–2 keV in Al. Being able to identify the energy of the non-thermal electrons directly from the underlying atomic physics largely replaces the need to assign a second temperature to the suprathermal tail of the electron distribution, an approach popular in laser-plasma interaction studies.

To unravel how such relatively low-energy hot electrons affect the emission spectrum, we start by modelling the heating process of a thin Al foil irradiated by x-rays at a photon energy of 1590 eV. This energy was deliberately chosen to be above the Al K-edge (1560 eV) so that the dominant absorption mechanism is

K-shell (1s) photoionization. The x-ray pulse is chosen to be a Gaussian in time with a FWHM duration of 40 fs, and has a spectral bandwidth of 0.4%, typical of a SASE FEL pulse. Four different intensities are compared, between  $2.5 \times 10^{15} \text{ Wcm}^{-2}$  and  $2.5 \times 10^{18} \text{ Wcm}^{-2}$ , depositing an ever increasing amount of energy into the target. Experimentally, these intensities would be realised by focusing the x-rays to various spot sizes: focusing the beam to a spot of a few micron in diameter typically yields intensities in region of  $10^{17} \text{ Wcm}^{-2}$  and can be readily achieved on most XFEL facilities.

We show the evolution of the electron density in Fig. 1, where we compare the results of the thermal and non-thermal models side by side. Snapshots in time of the same electron distribution are shown in Fig. 2. The x-ray pulse peaks in intensity in the middle of the simulation window, at 40 fs. The thermal simulations simply show a Maxwellian distribution that gets increasingly hotter in time over the duration of the excitation pulse. More deposited energy leads to increasing ionisation, and thus the free electron density also increases over time. The temperatures and densities are higher for higher irradiation intensities, since more energy is deposited into smaller volumes, as expected. The electron distribution function for the non-thermal simulation is visibly different, and can be divided into two components. The first is the bulk part of the free electron distribution, lying at lower energies. This assumes a near-Maxwellian shape because the electron thermalisation time is short even on the 100 fs timescales used here (see “Methods” section on the elastic collisional thermalisation model). This bulk component is largely equilibrated, and grows in prominence as the x-rays are absorbed and the sample heats. At higher energies, however, we can see a large energy spread over which non-thermal electrons can be found. These are mostly created by the equilibrating hot electrons generated in the x-ray-matter interaction process, and subsequent atomic kinetics. Two main sources of quasi-monoenergetic hot electrons can be identified: a feature at due to the photoionization of the Al L-shell electrons (at  $\approx 1520 \text{ eV}$ ), and a feature due to the Auger KLL process (at  $\approx 1420 \text{ eV}$ ) that efficiently fills a K-shell core hole. Both features can be readily seen in Figs. 1 and 2, but are clearest at the lowest intensities. They are harder to discern at high intensity because their relative populations, compared with the bulk free-electron distribution, decreases with intensity.

Figure 1 shows the density distribution on a logarithmic scale, and thus amplifies the non-thermal signature. But for the underlying physics, what matters most is the relative contribution of the quasi-thermalized component of the electron distribution in driving the atomic kinetics, compared with the non-thermal hot electron population. To examine this, we plot the populations for ionic charge states 3+ to 10+ in Fig. 3, in both the thermal and non-thermal case. We immediately note that the results are comparable: the charge state populations do not change dramatically under the instantaneous thermalisation approximation, validating this common assumption. Nevertheless, we do see a lag in the time at which certain charge states peak in the population distribution between the thermal and non-thermal calculations. In particular, we note that lower charge states in the more detailed non-thermal calculations tend to appear later in time compared with the thermal prediction, whereas higher charge states appear earlier in time. This is primarily due to the mechanism through which these charge states are created. The lower charge states are more efficiently generated via collisional ionisation processes driven by the bulk free electrons; these electrons heat up faster in the thermal calculation as all energy is placed into the thermal distribution instantaneously, whereas in the non-thermal case the bulk temperature rises more slowly as

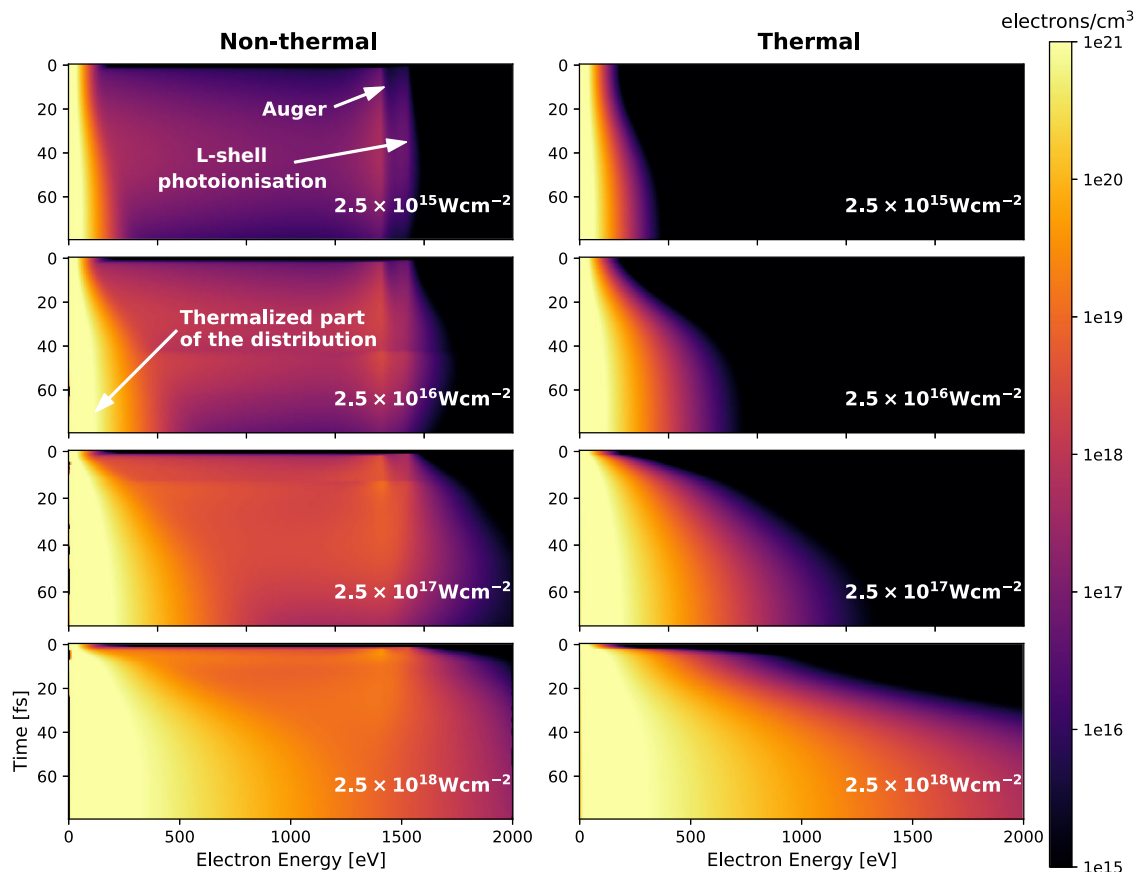


**Fig. 1** Thermal and non-thermal evolution of the electron distribution in Al irradiated by x-rays at 1590 eV. Non-thermal electrons generated from photoionization and Auger processes can be readily observed at higher energies in the non-thermal simulations, but are absent when assuming instantaneous thermalisation. The overall degree of heating is similar in the two cases.

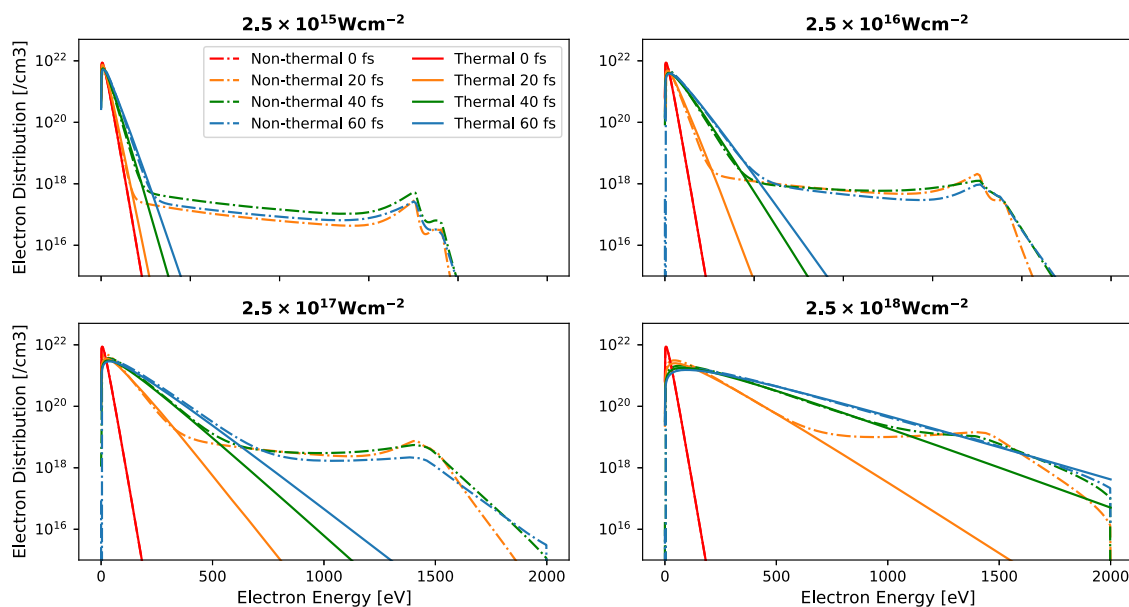


**Fig. 2** Snapshots in time of the electron distribution function shown in Fig. 1. The x-ray photon energy is 1590 eV in all cases. Because the non-thermal electrons are being continuously created by the FEL we observe a weak yet persistent tail in the distribution, which disappears only when subsumed by the thermal part of the distribution.

the energy needs to be transferred from the highly energetic photoionization and Auger electrons. In contrast, the higher charge states require substantially higher temperatures to be collisionally ionised, and are thus more efficiently created via

collisional interactions with the non-thermal electrons. Even if there are fewer of them available, they have sufficient energy to play an important, and possibly dominant role, in the dynamics of collisional ionisation.

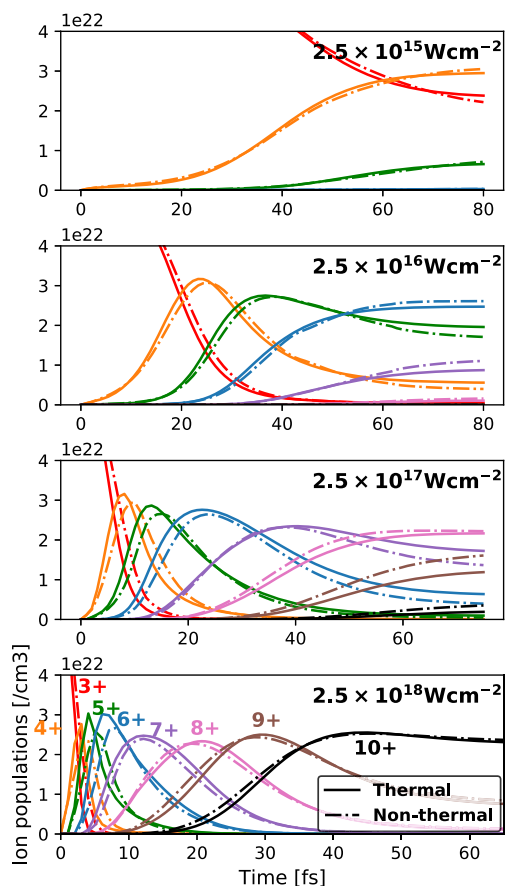


**Fig. 3** Effect of non-thermal electrons on the charge state populations in Al. The time evolution is computed for an x-ray photon energy of 1590 eV, a constant pulse duration of 40 fs, and for various pulse energies. This corresponds to a range of x-ray intensities on target.

In an experiment one cannot normally measure individual plasma charge state populations. However, these populations can be inferred via x-ray emission spectroscopy of  $K_{\alpha}$  satellite lines, when the sample is excited by x-rays above the relevant ionisation thresholds<sup>1,43</sup>. For charge states photo-pumped below their ionisation threshold, the appearance of emission lines can be instead indicative of collisional ionisation processes, and thus used to measure collisional rates<sup>33</sup>. For this measurement to be reliable, however, the bulk free electrons must be the dominant contributor to collisional ionisation, and the contributions from non-thermal electrons should be small.

We investigate the contribution of non-thermal electrons to the total  $K_{\alpha}$  emission spectrum in Fig. 4. The x-ray photon energy is set just above the K-edges of the first two charge states, but below the ionisation threshold of higher charge states. Thus only the first two charge states can be revealed directly via  $K_{\alpha}$  emission spectroscopy. While higher charge states are still present in the plasma, as illustrated in Fig. 3, their 1s states cannot be photo-ionised and they therefore cannot relax emitting a  $K_{\alpha}$  photon. Despite this, emission from higher charge states can still be observed, because of electron collisional ionisation of the L-shell in the presence of a K-shell hole<sup>36</sup>. Non-thermal electrons affect the emission spectrum in two key ways. Firstly, because the equilibration of photoionization and Auger electrons is the main heating channel of the bulk free-electron distribution, non-thermal electrons help determine the equilibration timescales and drive the evolution of the charge state population towards LTE. These evolving populations ultimately determine the emission

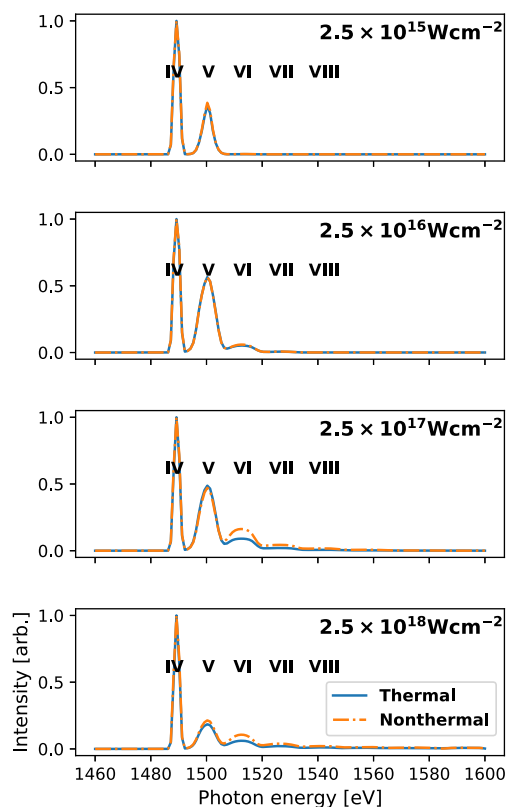


**Fig. 4** Effect of non-thermal electrons on the emission spectrum of Al.

The sample is irradiated by x-rays at 1590 eV at various peak intensities. At this photon energy the emission lines IV and V can be pumped directly via K-shell photoionization, while lines VI to VIII emit because of collisional processes. Discrepancies in the spectra start to appear at intensities above  $10^{17}$   $\text{Wcm}^{-2}$ .

intensity of charge states pumped above their K-edge thresholds. The second mechanism applies to charge states that are pumped below their K-shell ionisation threshold. These are primarily driven by collisional ionisation of the L-shell electrons, which can be either due to the bulk electrons at some average temperature  $k_B T \approx 100$  eV, or to the non-thermal electrons at a much higher energy (typically  $> 10 \times k_B T$ ). Higher electron energies are more efficient at L-shell ionisation, and so a system with a large non-thermal electron population and relatively cold bulk distribution will lead to more collisional ionisation, and consequently to more intense emission from higher charge states. We see this play out in the panels of Fig. 4. Because the x-ray pulse length is relatively long compared with the electron relaxation timescale, the thermal and non-thermal modelling predict very similar intensities for the first two emission lines. The charge state population is very close to LTE for intensities up to  $\sim 10^{18}$   $\text{Wcm}^{-2}$ , and the intensity of the first two lines is simply a reflection of the population of those charge states modulated by the temporal intensity of the x-ray pulse: the second charge state is most prominent at irradiation intensities of  $\sim 10^{16}$   $\text{Wcm}^{-2}$ , and decreases for lower (insufficient heating) and higher (too much heating) intensities. We note a slight difference in the intensity of the second line at the highest intensities: here the charge state is swept through very quickly, and the instantaneous thermalisation assumption starts to break down as it underestimates the time needed to establish LTE in the plasma distribution. The emission intensity of higher lines (VI and above) shows a considerably stronger dependence on the x-ray intensity. For intensities up to several times  $10^{16}$   $\text{Wcm}^{-2}$  the thermal and non-thermal predictions match,



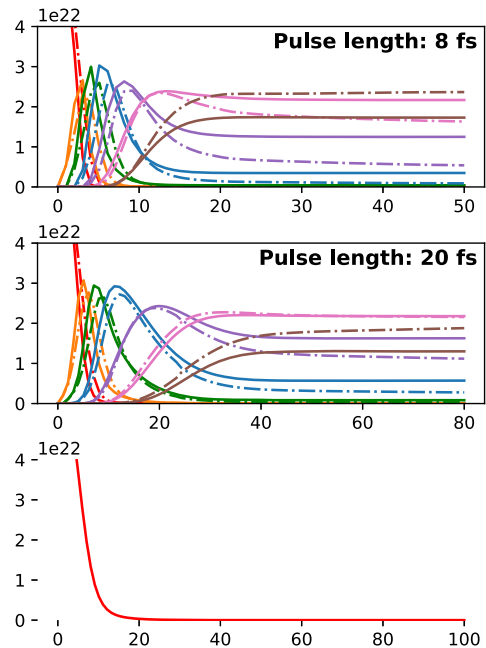
indicating that the L-shell ionisation process described above is indeed dominated by quasi-thermal bulk free electrons. Above this, the number of non-thermal electrons remains sufficiently high to more than double the effective ionisation rate, indicating a stark departure from LTE collisional dynamics.

The results shown in Fig. 4 are for a single x-ray intensity, and are thus not directly comparable with experimental results that are measured over a broad range of x-ray intensities. However, the average experimental intensity (rather than the often quoted peak intensity) is indicative of the overall irradiation regime, and can be linked to the discussion above. Average intensities typically achieved at the LCLS FEL, such as those fielded for the work on collisional ionisation presented in refs. <sup>33,36</sup>, is on the order of  $10^{16} \text{ Wcm}^{-2}$ .

**The effect of x-ray pulse length.** We have seen that for a given x-ray pulse duration, the effect of focusing the x-ray beam to achieve increasing intensities is to increase the relative contribution of non-thermal electrons to the evolution of the plasma, and thus to the observed emission spectrum. We now turn our attention to the effect of pulse length. Changing the pulse length is another way to change the intensity on target, but it adds an additional layer of complexity because the pulse duration also gates the observation timescale of the system. This is primarily because we only observe x-ray emission in the  $K_\alpha$  window when  $1s$  electrons can be ionised, and the overall temperatures reached in a typical microfocusing experiment ( $\approx 100 \text{ eV}$ ) are insufficient to drive collisional K-shell ionisation to any notable extent. Thus, emission is only observed during the x-ray pulse, and for a short time after depending on the femtosecond core-hole lifetime. By changing the duration of the x-ray pulse, while maintaining a constant pulse energy, we thus not only modify the x-ray intensity seen by the plasma, but also change the period over which we view the evolution of the charge state distribution. We show the simulated results for a Al plasma in Figs. 5 and 6. For these simulations we have assumed a pulse energy of 1 mJ, and a spotsize on-target of  $12 \mu\text{m}^2$ , so that a pulse length of 80 fs corresponds to an x-ray intensity of about  $10^{17} \text{ Wcm}^{-2}$ . These are typical values achievable at FEL facilities today<sup>1</sup>. The pulse energy is then kept constant, and the pulse duration lowered down to 8 fs.

For the longer pulse lengths of 40 and 80 fs we see little difference in the computed emission spectrum for the thermal and non-thermal cases, and a lag in the creation of various charge states analogous with that described in the previous section. In these cases, the observation window is sufficiently long for the evolution of the charge state populations to agree well with the assumption of instantaneous electron thermalisation. The overall population of the L-shell states is collisionally driven by the equilibrated bulk free electron distribution, and the charge states evolve as if in near-LTE for each point in time. For pulse durations of 20 fs and less, these assumptions start to break down, and the calculated spectrum assuming instantaneous electron thermalisation underestimates the emission intensity.

**Non-thermal electrons in resonant spectroscopy.** Recently, van den Berg et al. proposed driving a resonant  $1s \rightarrow 2p$  transition in Mg to measure collisional ionisation rates in dense plasmas<sup>36</sup>. The principle is straightforward: an x-ray pulse from a FEL is tuned to resonantly drive a specific inner-shell  $K_\alpha$  transition, and a spectroscopic measurement is performed to look for emission from neighbouring  $K_\alpha$  emission lines. Because of the narrow bandwidth of the FEL beam, the x-ray pulse can only excite a single  $K_\alpha$  line, and so the observation of multiple lines is indicative of L-shell collisional processes taking place during the



lifetime of a K-shell core hole. This method thus allows for a measurement of an ultra-fast collisional ionisation rate. However, the real objective is not so much to infer a rate, but rather to measure a collisional cross section. This can be accomplished using the expression in Eq. (1), under the caveat that the collisions are predominantly due to an interaction of the ion with the bulk free-electron distribution at some known temperature and density. But if the electron distribution is non-thermal, then it is easy to see that the cross section cannot uniquely be extracted from the integral expression of Eq. (1). Estimating the effect of non-thermal electrons is then important to guide the reliable interpretation of such experiments, especially since we have shown that the contribution of non-thermal electrons can be significant at high x-ray intensities, or for short x-ray pulse lengths.

For this investigation we set our simulation parameters to match the conditions of van den Berg et al.<sup>36</sup>: an optically thin Mg plasma at solid density is pumped at a photon energy of 1304 eV, corresponding to the resonance energy of the  $1s \rightarrow 2p$  transition energy in a  $7+$  Mg ion. At the nominal pulse duration of 60 fs the intensity on target is  $10^{17} \text{ Wcm}^{-2}$ . The collisional dynamics of interest take place at electron densities  $\sim 3 \times 10^{23} \text{ cm}^{-3}$  and temperatures of  $\sim 80 \text{ eV}$ . We show the evolution of the ionic populations as a function of time, using the thermal and a non-thermal models, in Fig. 7. The related emission spectra are shown in Fig. 8. Here we see that the assumption of instantaneous thermalisation holds well for nominal pulse durations, above  $\sim 30 \text{ fs}$ , providing a more rigorous justification of the assumptions

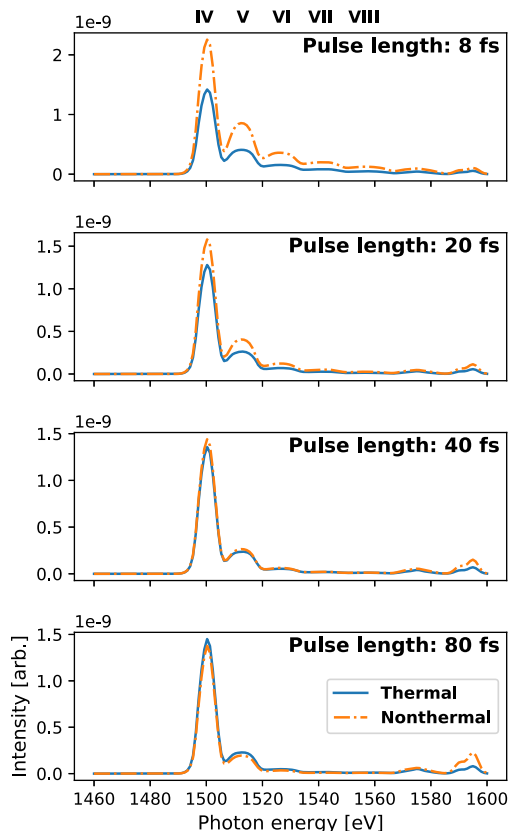


**Fig. 6 Effect of non-thermal electrons on the emission spectra of Al irradiated at constant energy for various pulse durations.** The ratio of the first two emission lines is very similar for pulses over 40 fs (where the peak of line V is ~15% of line IV), but starts to differ for shorter pulses. For the shortest 8 fs pulses line V is ~29% of line IV when instant thermalisation is assumed, but this ratio increases to 38% in the non-thermal simulation. The hot, non-thermal electrons enhance the overall emission by increasing the L-shell collisional ionisation rate.

made in the work on collisional ionisation rates. For shorter pulse durations the contribution of non-thermal electrons starts to become significant, and even dominant for pulse lengths below 10 fs. For these short pulses, modelling the full evolution of the electron distribution function becomes essential to produce atomic kinetics simulations with predictive capability.

When pumping a bound-bound transition on resonance the final ionisation state of the system depends strongly on the intensity of the x-ray irradiation, not just on the total energy in the pulse. This can be seen clearly in Fig. 7: for the shortest pulse durations of 6 fs the most populous charge states are 6+ and 7+, while for a 60 fs pulse length the 8+ dominates. This is mainly due to different temperatures – 6 fs is too short a time to substantially populate the resonant charge state which represents the dominant absorption channel. Longer pulses allow for the charge state to be populated collisionally, allowing for more resonant absorption and isochoric heating. In contrast, systems heated by x-rays above an ionisation threshold show a much weaker dependence on the intensity, as can be readily seen in Fig. 5: the most populous charge states are between 8+ and 9+ for all pulse durations between 8 fs and 80 fs. Notably, the population of charge states is predominantly driven by the thermal electrons, and is thus captured well by the thermal calculations. The same cannot be said for the emission spectra, which show a more pronounced, and experimentally observable,

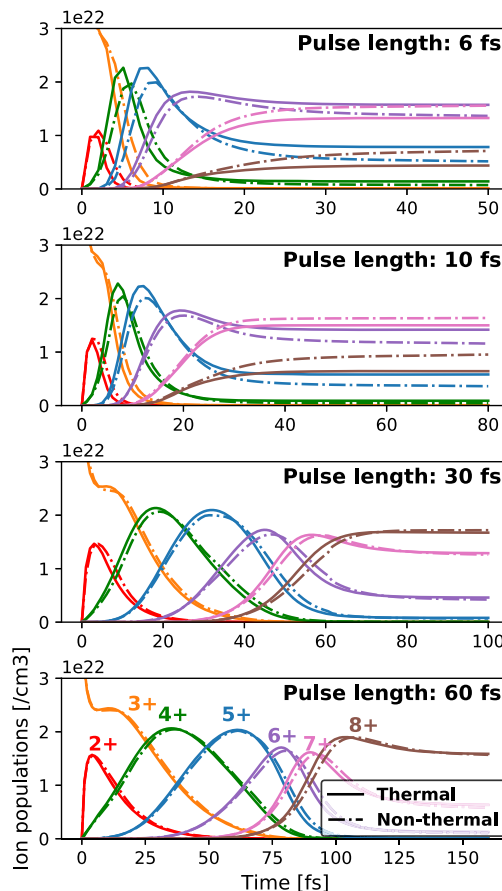


**Fig. 7 Thermal (solid) and non-thermal (dot-dashed) evolution of the charge state populations in resonantly pumped Mg.** The sample is irradiated on-resonance at 1304 eV, at constant energy, and for various pulse lengths.

dependence on non-thermal electron collisions for short pulse durations.

### Conclusions

We have presented the atomic kinetics simulation package CCFLY, which can model the non-thermal (electron) and non-LTE (ion) evolution of matter interacting with intense x-ray radiation on ultra-short timescales. We have used these capabilities to investigate the evolution of solid-density systems, heated isochorically to high temperatures via femtosecond FEL pulses, and assess the role of non-thermal electron distributions. We find that in mid-Z systems such as Al and Mg, non-thermal electrons become important in determining the short-time plasma kinetics and electron dynamics for intensities above  $10^{17} \text{ W cm}^{-2}$ , and for pulse lengths below 10 fs.

To date, the use of Fokker-Planck models within collisional-radiative simulations to interpret experiments at free-electron lasers has been limited, largely due to the substantial computational cost the method requires. Whilst we have shown that this is justifiable for experiments using a typical SASE FEL pulse duration of ~50 fs, ongoing developments enabling the routine generation of energetic few-fs and sub-fs pulses, and of ultra-high intensities via narrow bandwidth self-seeding and x-ray nanofocusing, are increasingly accessing x-ray regimes where the direct modelling of non-thermal electron relaxation will be essential to retain predictive power in the modelling of extreme x-ray matter interactions.

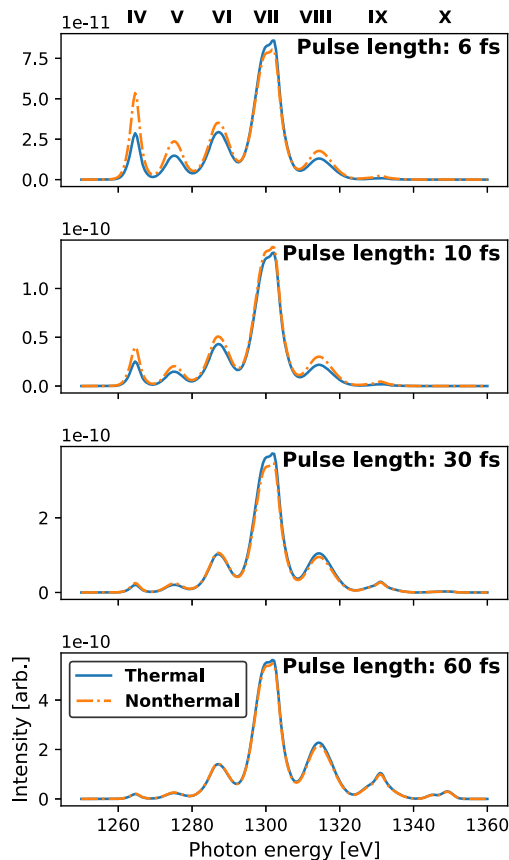


**Fig. 8 Effect of non-thermal electrons on the emission spectra of resonantly pumped Mg.** Mg is irradiated on-resonance at 1304 eV, at constant energy, and for various pulse lengths. The emission lines on both sides of the resonant VII  $K_{\alpha}$  line are due to collisional ionisation (to higher energies) and three-body recombination (to lower energies). Non-thermal electrons start to affect the spectrum for pulse lengths below 30 fs.

## Methods

**The CCFLY atomic kinetics model.** The evolution of our system is described in terms of the changes in the relative population density  $N_i(t)$  of each ionic charge state (labelled by the index  $i$ ), and of the free electron distribution  $f_E(E, t)$ . A collisionally-induced transition between two ion states given by some cross section  $\sigma_{\pm}(E)$  is described in the model by a transition rate per unit volume  $S^{\pm}(t)/V$  given by

$$S^{\pm}(t)/V = \int \sqrt{2E/m_e} \sigma_{\pm}(E) f_E(E, t) dE, \quad (1)$$

where  $E$  is the kinetic energy of the electron and  $m_e$  the electron mass. By computing the transition rates between all the ion states, we can construct a transition matrix  $S$ . For each available ion state  $i$ , its population density  $N_i$  can then be determined by the following set of coupled rate equations

$$\frac{dN_i(t+dt) - N_i(t)}{dt} = N_i(t) \left( \sum_{j \neq i} S_{ji} - \sum_{k \neq i} S_{ik} \right). \quad (2)$$

Because our system is globally neutral, the total electron density  $N_e$  can be calculated from the ion density and the ionisation  $z$  as:

$$N_e(t+dt) = \sum_i N_i(t+dt) z_i, \quad (3)$$

where we have summed across all ion states and multiplied them by their ionisation  $z_i$ . From the perspective of energy balance, the ion transitions can either add energy or draw energy from the free electron population. Thus, due to the requirement of energy conservation, the energy change in the free electron distribution is given by:

$$\frac{dE_{\text{kin}}(t)}{dt} = - \sum_{i \neq j} S_{ij} E_{ij} N_i(t) + \frac{dE_{\text{rad}}(t)}{dt}, \quad (4)$$

where  $E_{ij}$  is the energy difference in between ionic charge states  $i$  and  $j$  involved in the transition  $i \rightarrow j$ . This expression sums up all the energies that are released into, or drawn from, the free electron distribution due to photo-absorption, Auger decay, and collisional interactions. This includes bound-bound radiative

transitions, bound-bound collisional transitions, bound-free radiative ionisation, bound-free radiative recombination, bound-free collisional ionisation, bound-free collisional recombination, autoionization, and electron capture.

We will call the model thermal if we assume that the electron distribution function is Maxwellian, uniquely described by an electron density  $N_e$  and a temperature  $T$ . For situations where energy is entering the system, for example via x-ray photoabsorption, the temperature and density are instantaneously equilibrated at each time step. Then,

$$\frac{3}{2} N_e(t) k_B T(t) = E_{\text{kin}}(t). \quad (5)$$

In this case, Eqs. (3) and (4) completely determine the free-electron distribution in terms of the changing temperature and density of the ionised electrons.

In contrast, if a thermal electron distribution cannot be assumed, then the change in the electron distribution needs to be modelled explicitly for all electron energies. This can be accomplished using the Fokker–Planck equation:

$$\left. \frac{\partial f_E(E)}{\partial t} \right|_{ee} = - \frac{\partial}{\partial E} [a(E) f_E(E)] + \frac{1}{2} \frac{\partial^2}{\partial E^2} [D(E) f_E(E)] + I(f_E(E)) + S(E). \quad (6)$$

The change in the electron distribution as a function of time is governed by four terms on the right hand side of this equation. The first two terms, containing  $a(E)$  and  $D(E)$ , describe the elastic part of the evolution. The third term  $I(f_E(E))$  denotes all contributions of inelastic collisional processes within the electron distribution, where the free electrons either gain or lose energy to the ionic charge state. The last term  $S(E)$  denotes the collection of all source interactions that do not depend on the electron distribution. By capturing the effects on the electron distribution in an inelastic collision operator that considers the photo-ionisation and Auger decay, a self-consistent approach for the ion populations and electrons can be achieved. Then the ionic charge state populations, the electron distribution and its time-derivatives can be fed into an ordinary differential equation (ODE) solver. We refer to this situation as the non-thermal case.

CCFLY supports two levels of detail in the atomic data used in the atomic kinetics modelling: superconfigurations and relativistic configurations. In the super-configurational approach, we simply count how many electrons are bound with each quantum number. States are denoted in the  $K_a L_b M_c N_d$  notation which means that there are  $a$  electrons in the K-shell ( $n=1$ ),  $b$  electrons in the L-shell ( $n=2$ ),  $c$  electrons in the M-shell ( $n=3$ ) and  $d$  electrons in the N-shell ( $n=4$ ). The advantage of using superconfigurations is that the dataset can be kept relatively small compared with a more detailed configurations dataset. In contrast, relativistic configurations provide access to more detailed atomic physics modelling, but at a substantially greater computational cost. A relativistic configurations dataset can be generated using the Flexible Atomic Code<sup>44,45</sup>, via the CFACDB library that provides access to the cFAC-generated databases.

**Elastic electron collisions.** The elastic part of the evolution of the electron distribution is given by the first two terms in the Fokker Planck equation in Eq. (6). The elastic collision terms can alter the shape of the distribution, while preserving particle density and total kinetic energy. Additionally, the distribution function should equilibrate to the correct Maxwellian distribution. In CCFLY, the electron distribution is initialised and evolved in energy space but in the Fokker–Planck operator, the electrons are evolved in velocity space. First derived by Bobylev and Chuyanov<sup>46</sup>, and cast into a non-relativistic collision operator by Tzoufras et al.<sup>47,48</sup>, this formulation is given in integro-differential operator form as:

$$\left( \frac{\partial f_v(v)}{\partial t} \right)_{ee} = \frac{4\pi\Gamma_{ee}}{3} \frac{1}{v^2} \frac{\partial}{\partial v} \left[ \frac{1}{v} \frac{\partial W(v)}{\partial v} \right], \quad (7)$$

where the function  $W(v)$  is given by:

$$W(v) = f_v \int_0^v f_u u^4 du + v^3 f_v \int_v^\infty f_u u du - 3 \int_v^\infty f_u u du \int_0^v f_u u^2 du. \quad (8)$$

The function  $W(v)$  contains the time evolution of the electron distribution due to to electron-electron collisions that conserve particle number and kinetic energy. The  $\Gamma_{ee}$  term is defined as:

$$\Gamma_{ee} = \frac{e^4 \ln \Lambda}{4\pi\epsilon_0^2 m_e^2}, \quad (9)$$

with  $e$  the electron charge, and  $\ln \Lambda$  the Coulomb logarithm. The Coulomb logarithm for electron-electron interactions in hot plasmas is computed with a semi-empirical formula constructed by Huba<sup>49</sup>:

$$\ln \Lambda = 23.5 - \ln \left( N_e^{1/2} T^{-5/4} \right) - \left[ 10^{-5} + (\ln T - 2)^2 / 16 \right]^{1/2}, \quad (10)$$

where the density and temperature have units of  $\text{cm}^{-3}$  and eV, respectively.

For large velocities, Eq. (8) can be evaluated through standard discretisation techniques such as the chained trapezoid method. For velocities that are small compared with the characteristic velocity  $v_e$  of the distribution, the second and third term in Eq. (8) cancel up to  $\mathcal{O}(v^3)$ . It is necessary to modify the numerical scheme to capture this, in order for the distribution to equilibrate to a Maxwellian. This can be done by writing  $W(v_n)$  as a Taylor series  $f_n \approx f(0) + [f_1 - f(0)](v_n^2/v_1^2)$  and  $f(0) = (f_0 - f_1 v_0^2/v_1^2)/(1 - v_0^2/v_1^2)$ . Setting



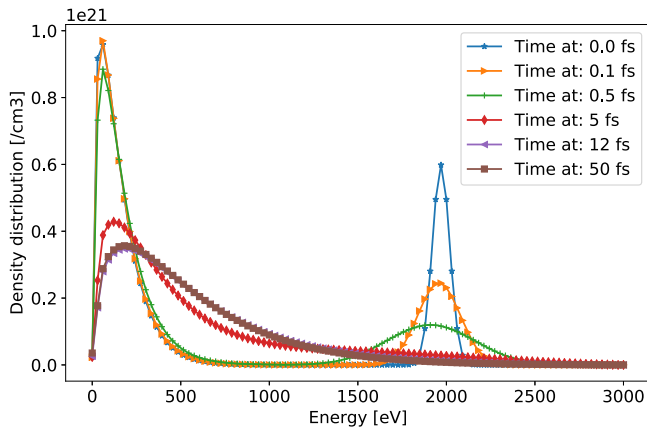


**Fig. 9 Modelling of elastic collisional thermalisation.** We initialise a non-thermal distribution consisting of a Maxwellian and an additional hot-electron spike centred at 2 keV. The distribution equilibrates collisionally on a timescale of  $\sim 10$  fs.

$W(v_n < v_c) \equiv W_s(v)$ , this results in:

$$W_s(v) = f_n \times \left[ f(0) \frac{v_n^5}{5} + (f_1 - f(0)) \frac{v_n^7}{7v_1^2} \right] + \left[ (f_n - f(0))v_n^3 - (f_1 - f(0)) \frac{3v_n^5}{5v_1^2} \right] \times \sum_{k=n+1}^{N-1} \frac{1}{2} (f_k v_k + f_{k-1} v_{k-1}) \delta_{k-1/2}. \quad (11)$$

Similarly, setting  $W(v_n \geq v_c) \equiv W_l(v)$ , we have

$$W_l(v) = f_n \sum_{k=0}^n \frac{1}{2} (f_k v_k^4 + f_{k-1} v_{k-1}^4) \delta_{k-1/2} + v_n^3 f_n \sum_{k=n+1}^{N-1} \frac{1}{2} (f_k v_k + f_{k-1} v_{k-1}) \delta_{k-1/2} - 3 \left[ \sum_{k=n+1}^{N-1} \frac{1}{2} (f_k v_k + f_{k-1} v_{k-1}) \delta_{k-1/2} \right] \times \left[ \sum_{k=1}^n \frac{1}{2} (f_k v_k^2 + f_{k-1} v_{k-1}^2) \delta_{k-1/2} \right]. \quad (12)$$

We show an example of how this elastic collisional operator relaxes a non-thermal electron distribution to a Maxwellian in Fig. 9. For simplicity, we assume here that only free electrons are involved in the collisional thermalisation process, and all interactions with ions (e.g. collisional ionisation and recombination) are ignored. We initialise the electrons to a thermal distribution at 100 eV, and add an additional non-thermal population of electrons with energies centred at 2 keV. The collisional operator equilibrates the distribution to a new overall temperature of 365 eV within some 10 femtoseconds.

Because we equilibrate the free electrons to a Maxwell-Boltzmann rather than to a Fermi-Dirac distribution, our model (and our collision rates, in particular) will be inaccurate for temperatures below the Fermi temperature

$$T_F = \frac{\hbar^2}{2k_B m_e} (3\pi^2 n_e)^{2/3}, \quad (13)$$

where  $n_e$  denotes the electron density. At the solid densities considered here, this corresponds to temperatures in the region of 5–10 eV. Because of this, we initialise our simulations at a temperature of  $3/5 E_F$ , corresponding to the mean energy of an electron in a Fermi-Dirac distribution at  $T = 0$ , and start the evolution from there. The x-rays must isochothermally heat the system beyond the Fermi energy within the first few time steps to justify this modelling approach. One might assume that it is this lack of a Fermi-Dirac implementation which fundamentally limits our modelling to relatively hot systems. However, this is only partially correct: in reality, the entire collisional-radiative modelling infrastructure presented in this section is based on a classical picture of electron-ion and electron-electron binary collisional processes, and on the atomic structure of isolated atoms, neither of which necessarily converges to known results in the condensed matter limit at low temperatures. We do not seek to address these challenging issues here, and instead choose to restrict our modelling to systems at temperatures considerably above the Fermi temperature throughout our investigations.

## Data availability

The data presented in this work is available upon reasonable request.

## Code availability

Access to the code may be made upon reasonable request, where permissible.

Received: 4 August 2022; Accepted: 25 April 2023;  
Published online: 10 May 2023

## References

- Vinko, S. M. et al. Creation and diagnosis of a solid-density plasma with an x-ray free-electron laser. *Nature* **482**, 59–62 (2012).
- Fletcher, L. B. et al. Ultrabright x-ray laser scattering for dynamic warm dense matter physics. *Nat. Photon.* **9**, 274–279 (2015).
- Levy, A. et al. The creation of large-volume, gradient-free warm dense matter with an x-ray free-electron laser. *Phys. Plasmas* **22**, 030703 (2015).
- Ciricosta, O. et al. Detailed model for hot-dense aluminum plasmas generated by an x-ray free electron laser. *Phys. Plasmas* **23**, 022707 (2016).
- Ciricosta, O. et al. Direct measurements of the ionization potential depression in a dense plasma. *Phys. Rev. Lett.* **109**, 065002 (2012).
- Vinko, S. M., Ciricosta, O. & Wark, J. S. Density functional theory calculations of continuum lowering in strongly coupled plasmas. *Nat. Commun.* **5**, 3533 (2014).
- Kasim, M. F. et al. Inverse problem instabilities in large-scale modeling of matter in extreme conditions. *Phys. Plasmas* **26**, 112706 (2019).
- Eggert, J. H. et al. Melting temperature of diamond at ultrahigh pressure. *Nat. Phys.* **6**, 40–43 (2010).
- Smith, R. F. et al. Equation of state of iron under core conditions of large rocky exoplanets. *Nat. Astron.* **2**, 452–458 (2018).
- Gaffney, J. et al. A review of equation-of-state models for inertial confinement fusion materials. *High. Energy Density Phys.* **28**, 7–24 (2018).
- Toleikis, S. et al. Probing near-solid density plasmas using soft x-ray scattering. *J. Phys. B: At. Mol. Opt. Phys.* **43**, 194017 (2010).
- Chung, H.-K. et al. Atomic processes modeling of x-ray free electron laser produced plasmas using SCFLY code. *AIP Conf. Proc.* **1811**, 020001 (2017).
- Vinko, S. M. et al. Electronic structure of an XUV photogenerated solid-density aluminum plasma. *Phys. Rev. Lett.* **104**, 225001 (2010).
- Medvedev, N., Zastra, U., Förster, E., Gericke, D. O. & Rethfeld, B. Short-time electron dynamics in aluminum excited by femtosecond extreme ultraviolet radiation. *Phys. Rev. Lett.* **107**, 165003 (2011).
- Preston, T. R. et al. Measurements of the K-shell opacity of a solid-density magnesium plasma heated by an x-ray free-electron laser. *Phys. Rev. Lett.* **119**, 085001 (2017).
- Milder, A. L., Ivancic, S. T., Palastro, J. P. & Froula, D. H. Impact of non-maxwellian electron velocity distribution functions on inferred plasma parameters in collective thomson scattering. *Phys. Plasmas* **26**, 022711 (2019).
- de la Varga, A. G. et al. Non-maxwellian electron distributions in time-dependent simulations of low- $z$  materials illuminated by a high-intensity x-ray laser. *High. Energy Density Phys.* **9**, 542–547 (2013).
- Sentoku, Y. & Kemp, A. Numerical methods for particle simulations at extreme densities and temperatures: Weighted particles, relativistic collisions and reduced currents. *J. Comput. Phys.* **227**, 6846–6861 (2008).
- Sentoku, Y., Parashiv, I., Royle, R., Mancini, R. C. & Johzaki, T. Kinetic effects and nonlinear heating in intense x-ray-laser-produced carbon plasmas. *Phys. Rev. E* **90**, 051102 (2014).
- Royle, R., Sentoku, Y., Mancini, R. C., Parashiv, I. & Johzaki, T. Kinetic modeling of x-ray laser-driven solid al plasmas via particle-in-cell simulation. *Phys. Rev. E* **95**, 063203 (2017).
- Le, H. P., Sherlock, M. & Scott, H. A. Influence of atomic kinetics on inverse bremsstrahlung heating and nonlocal thermal transport. *Phys. Rev. E* **100**, 013202 (2019).
- Abdallah, J., Colgan, J. & Rohringer, N. Time-dependent calculations of electron energy distribution functions for neon gas in the presence of intense xfel radiation. *J. Phys. B: At. Mol. Opt. Phys.* **46**, 235004 (2013).
- Chung, H.-K., Chen, M. & Lee, R. Extension of atomic configuration sets of the non-lte model in the application to the  $k\alpha$  diagnostics of hot dense matter. *High. Energy Density Phys.* **3**, 57–64 (2007).
- Chung, H.-K., Chen, M., Morgan, W., Ralchenko, Y. & Lee, R. FLYCHK: Generalized population kinetics and spectral model for rapid spectroscopic analysis for all elements. *High. Energy Density Phys.* **1**, 3–12 (2005).
- Cho, B. I. et al. Electronic structure of warm dense copper studied by ultrafast x-ray absorption spectroscopy. *Phys. Rev. Lett.* **106**, 167601 (2011).
- Vinko, S. M. et al. Time-resolved XUV opacity measurements of warm dense aluminum. *Phys. Rev. Lett.* **124**, 225002 (2020).
- Lee, J.-W. et al. Investigation of nonequilibrium electronic dynamics of warm dense copper with femtosecond x-ray absorption spectroscopy. *Phys. Rev. Lett.* **127**, 175003 (2021).
- Zhang, J., Qin, R., Zhu, W. & Vorberger, J. Energy relaxation and electron and phonon coupling in laser-excited metals. *Materials* **15**, 1902 (2022).
- Andreasson, J. et al. Saturated ablation in metal hydrides and acceleration of protons and deuterons to keV energies with a soft-x-ray laser. *Phys. Rev. E* **83**, 016403 (2011).

30. Cho, B. I. et al. Resonant  $K\alpha$  spectroscopy of solid-density aluminum plasmas. *Phys. Rev. Lett.* **109**, 245003 (2012).
31. Brown, C. R. D. et al. Evidence for a glassy state in strongly driven carbon. *Sci. Rep.* **4**, 5214 (2014).
32. Rackstraw, D. et al. Opacity effects in a solid-density aluminium plasma created by photo-excitation with an x-ray laser. *High. Energy Density Phys.* **11**, 59–69 (2014).
33. Vinko, S. M. et al. Investigation of femtosecond collisional ionization rates in a solid-density aluminium plasma. *Nat. Commun.* **6**, 6397 (2015).
34. Ciricosta, O. et al. Measurements of continuum lowering in solid-density plasmas created from elements and compounds. *Nat. Commun.* **7**, 11713 (2016).
35. Kasim, M. F., Wark, J. S. & Vinko, S. M. Validating continuum lowering models via multi-wavelength measurements of integrated x-ray emission. *Sci. Rep.* **8**, 6276 (2018).
36. van den Berg, Q. Y. et al. Clocking femtosecond collisional dynamics via resonant x-ray spectroscopy. *Phys. Rev. Lett.* **120**, 055002 (2018).
37. Griem, H. R. *Principles of Plasma Spectroscopy*. Cambridge Monographs on Plasma Physics (Cambridge University Press, 1997).
38. Chen, M. H., Crasemann, B. & Mark, H. Relativistic K-shell auger rates, level widths, and fluorescence yields. *Phys. Rev. A* **21**, 436–441 (1980).
39. Chung, H.-K., Hansen, S. B. & Scott, H. A. *Modern Methods in Collisional-Radiative Modeling of Plasmas* (Springer, 2016).
40. Preston, T. R. et al. The effects of ionization potential depression on the spectra emitted by hot dense aluminium plasmas. *High. Energy Density Phys.* **9**, 258–263 (2013).
41. Rosmej, F. B. Hot electron x-ray diagnostics. *J. Phys. B: At., Mol. Opt. Phys.* **30**, L819 (1997).
42. Glenzer, S. H. et al. Measurements of suprathermal electrons in hohlraum plasmas with x-ray spectroscopy. *Phys. Rev. Lett.* **81**, 365–368 (1998).
43. Vinko, S. M. X-ray free-electron laser studies of dense plasmas. *J. Plasma Phys.* **81**, 365810501 (2015).
44. Gu, M. F. The flexible atomic code. *Can. J. Phys.* **86**, 675–689 (2008).
45. Gu, M. F. The flexible atomic code. *AIP Conf. Proc.* **730**, 127–136 (2004).
46. Bobylev, A. & Chuyanov, V. On the numerical solution of Landau's kinetic equation. *USSR Comput. Math. Math. Phys.* **16**, 121–130 (1976).
47. Tzoufras, M., Bell, A. R., Norreys, P. A. & Tsung, F. S. A vlasov-fokker-planck code for high energy density physics. *J. Comput. Phys.* **230**, 6475–6494 (2011).
48. Tzoufras, M., Tableman, A., Tsung, F. S., Mori, W. B. & Bell, A. R. A multi-dimensional Vlasov-Fokker-Planck code for arbitrarily anisotropic high-energy-density plasmas. *Phys. Plasmas* **20**, 056303 (2013).
49. Huba, J. D. *NRL PLASMA FORMULARY Supported by The Office of Naval Research*. (Naval Research Laboratory, 2013).

## Acknowledgements

S.R., M.F.K., J.S.W. and S.M.V. acknowledge support from the UK EPSRC grants EP/P015794/1 and EP/W010097/1, and from the Royal Society. P.V. acknowledges support from the Spanish MICINN grant PID2021-124129OB-I00. S.M.V. is a Royal Society University Research Fellow.

## Author contributions

S.R., Q.Y.vdB., M.K., H.-K.C., J.S.W. and S.M.V. contributed to the development of the CCFLY code. S.R., Q.Y.vdB., Y.S., H.-K.C., E.V.F.-T. and P.V. developed the non-thermal module. S.R. and Y.S. performed the simulations. S.R. and S.M.V. conceived the project and wrote the manuscript, with contributions from all authors.

## Competing interests

The authors declare no competing interests.

## Additional information

**Correspondence** and requests for materials should be addressed to Sam M. Vinko.

**Peer review information** *Communications Physics* thanks Istvan Foldes and the other, anonymous, reviewer(s) for their contribution to the peer review of this work.

**Reprints and permission information** is available at <http://www.nature.com/reprints>

**Publisher's note** Springer Nature remains neutral with regard to jurisdictional claims in published maps and institutional affiliations.



**Open Access** This article is licensed under a Creative Commons Attribution 4.0 International License, which permits use, sharing, adaptation, distribution and reproduction in any medium or format, as long as you give appropriate credit to the original author(s) and the source, provide a link to the Creative Commons license, and indicate if changes were made. The images or other third party material in this article are included in the article's Creative Commons license, unless indicated otherwise in a credit line to the material. If material is not included in the article's Creative Commons license and your intended use is not permitted by statutory regulation or exceeds the permitted use, you will need to obtain permission directly from the copyright holder. To view a copy of this license, visit <http://creativecommons.org/licenses/by/4.0/>.

© The Author(s) 2023